Fatigue life optimization for 17-4Ph steel produced by selective laser melting

Jean-Marc Linares, Julien Chaves-Jacob, Quentin Lopez, Jean-Michel Sprauel

Linares, J. M., Chaves-Jacob, J., Lopez, Q., & Sprauel, J. M. (2022). Fatigue life optimization for 17-4Ph steel produced by selective laser melting. *Rapid Prototyping Journal*.

Fatigue life optimization for 17-4Ph steel produced by selective laser melting

Linares, Jean-Marc, Chaves-Jacob, Julein, Lopez, Quentin, & Sprauel, Jean-Michel
Aix-Marseille Université, CNRS, ISM UMR, Marseille, France

Abstract:
Purpose: The mechanical characterization of Selective Laser Melting (SLM) parts is an industrial challenge. In this paper, a methodology is proposed to control the fatigue life of 17-4Ph stainless steel by selecting the most relevant manufacturing parameters: i.e., laser power, laser travel speed, hatch spacing and laser defocusing.
Design/methodology/approach: A rough and a refined Design Of Experiment (DOE) are carried out to target the best combination of process parameters. A response surface model is then constructed to predict the parameter combination that optimizes the fatigue performance.
Findings: Our results show that the fatigue limit of the specimens manufactured by SLM (471.7 MPa at 10^7 cycles) has reached near 90% of the value found in samples machined from a bar. This demonstrates the applicability of the method proposed to optimize SLM process and control the fatigue life of 17-4Ph stainless steel. Our results are compared to other research works and provide an increase of 18% to the fatigue limit.
Originality: This research work showcases a DOE methodology to optimize the SLM parameters to achieve fatigue performance as great as that of solid 17-4Ph stainless steel.
Keywords: Additive manufacturing, Selective laser melting, 17-4 Ph stainless steel, Fatigue, Residual stress, Deformation, Material
Paper type: Research paper

1. Introduction

Additive manufacturing opens new opportunities to manufacture a mechanical part (Thompson et al., 2016) regardless of its geometrical complexity (Schmidt et al., 2017). Laser Beam Powder Bed Fusion (LB-PBF) technologies, developed for metal deposition, can be classified in 2 subgroups: Selective Laser Melting (SLM) and Electron Beam Melting (EBM). The control of the mechanical properties of workpiece material obtained by these manufacturing processes is an industrial challenge. The fatigue performance of parts produced by LB-PBF technology is a hot topic for mechanical industries (Yadollahi and Shamsaei, 2017), particularly, in aeronautic sector. Figure 1 summarizes the state of the art about fatigue performance of parts manufactured by LB-PBF. Fatigue life can be influenced by a great number of parameters. In figure 1, in accordance with the literature, the most influential parameters were classified into 5 groups (machine setup parameters, part position, build orientation, workspace inert gas, powder re-use). During LB-PBF deposition process, the material and the part are built simultaneously, using these parameters. In the literature, four characteristics that control the material fatigue behaviour have been identified: material structure, deformation/residual stress, defect/porosity, and surface roughness. These characteristics are included in figure 1. This state-of-the-art of the process focuses on 17-4Ph stainless steel which is a material used in the aeronautic sector and is the object of our study.

Recently, the effects on the 17-4Ph fatigue performance of surface quality and sub-surface porosity were studied (Romano et al., 2020). The authors concluded that the presence of porosity near the surface has a negative effect on the material fatigue performance. Previous studies have highlighted the influence of the surface roughness and of the porosity on the fatigue properties for other materials.

These studies showed the sensitivity of the additive manufacturing machine parameters onto the resulting roughness quality and porosity (Tian et al., 2017; Gockel et al., 2019).

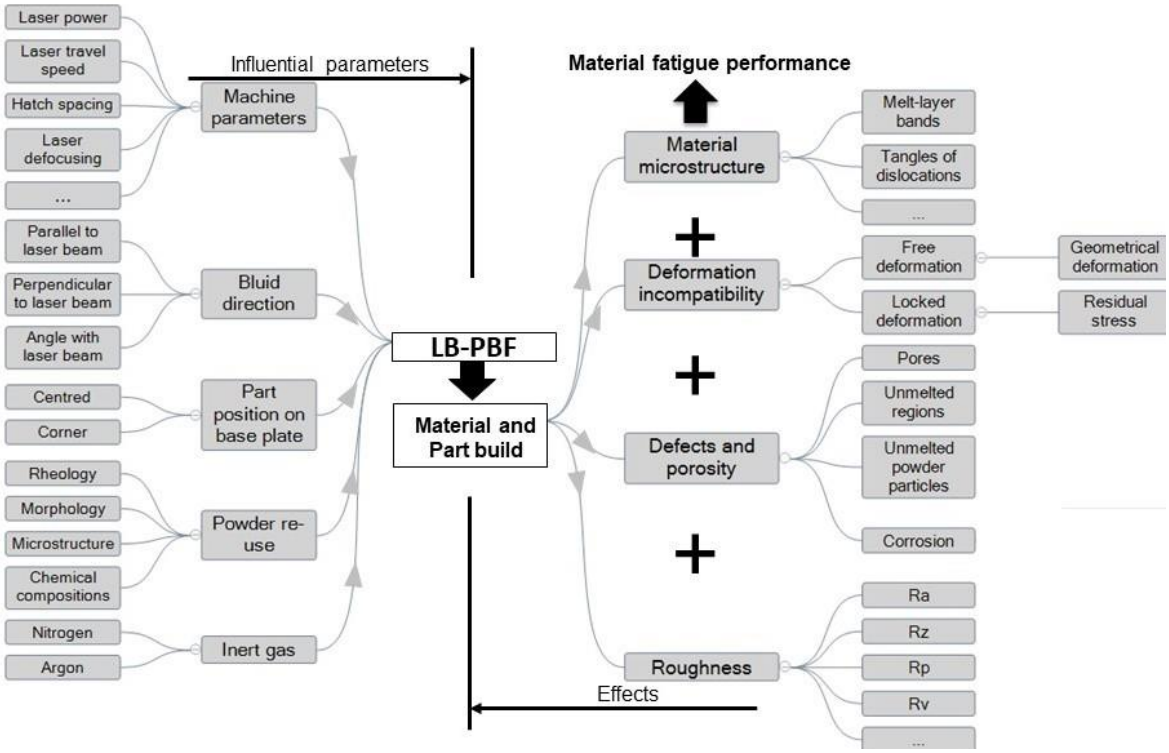

Figure 1 State of the art of material fatigue performance for parts manufactured by LB-PBF technology.

In the works dealing with the fatigue behaviour of selective laser melted 17-4Ph, the impact of the part building orientation and its position on the base plate was also considered. The results highlighted that:

- specimens produced in horizontal position have higher fatigue life than those placed vertically (Yadollahi et al., 2017),

- in the case of powder re-use, the decrease of the number of fine particles and the manufactured part location on the base plate have a great influence on the fatigue behaviour. The fatigue life is also impacted by the morphology of grains, the rheology, and the alteration of the powder microstructure when re-used (Dobson and Starr, 2021; Soltani-Tehrani et al., 2020).

The improvement of microstructural quality is an active research field for 17-4Ph steel (Nezhadfar et al. 2019a; Nezhadfar et al. 2019b). Metastable austenite's role in the mechanical behaviour of additive manufactured part was studied (Lebrun et al., 2015). The authors recommend carrying out a post heat treatment to eliminate the retained austenite in the material. H1025 and H1150 heat treatments should be used to reduce the residual stresses. This also allows to transform the austenite into martensite during cooling. Parts manufactured by SLM process present a texture in the build direction (Murret al., 2012; Mahmoudi et al., 2017). Perpendicular to this direction, the material exhibits dense entanglement of dislocations. This anisotropy of the material is detrimental to the fatigue performance. Another work (Alnajjar et al., 2020) showed that 17-4Ph produced by additive manufacturing is susceptible to hydrogen embrittlement. One more study highlighted the impact of surface porosity in case of salt corrosion (Schaller et al., 2017). Furthermore, fatigue behaviour of 17-4Ph parts produced by additive manufacturing was intensively studied in research works (Yadollahi and Shamsaei, 2017; Carneiro et al., 2019).

Many research works were completed on LB-PBF technology to control the quality of the deposited material (Bourell et al., 2017). The LB-PBF process relies on a great number of parameters (e.g., material, LB-PBF machine technology, and setup parameters). The material deposition principle

of LB-PBF technology is close to the physical process used in overlay welding (OW): interaction between a thermal source (laser or electron sources) and a material (deposited metal and metallic powder). In OW or LB-PBF process, controlling the material integrity is crucial to get a high fatigue life of manufactured parts. The metallurgical properties of deposited material are key parameters to master the material integrity. Each material has specific phase transformations which require the manufacturing parameters of LB-PBF machine to be accurately adjusted. It is the case, for example, of 17-4Ph stainless steel which is a premium, precipitation-hardened martensitic stainless steel designed primarily to be used in aircraft and space industry. Its main properties are high strength and corrosion resistance (ultimate tensile strength of 800 to 1300 MPa, hardness of 42 HRC depending on heat treatments). It is used in the manufacturing of parts which require both high strength and high toughness.

Given that the SLM process is a complex and multi-physics process, it is difficult to build a physical model that factors in all the phenomena involved in this process. Therefore, in this paper, a DOE methodology is presented to optimize the SLM manufacturing parameters in order to increase the fatigue life of 17-4Ph stainless steel. We assume that this fatigue life is linked to a high material integrity. In this study, a first DOE was carried out to determine the adequate SLM process parameters that would increase the material integrity of 17-4Ph. The second step of our method focused on the reduction of the geometric deformations of the parts in order to limit the collisions between the recoater (SLM machine used in this study has a rigid deposition system: steel roller) and the part on the SLM Machine. For this, a second DOE was carried out. To conclude this study, fatigue tests were carried out comparatively between specimens produced by SLM and machined from bar. Thus, five raw fatigue test specimens were manufactured by SLM, using the optimized parameters, and then finished by turning. Five other samples were machined from a 17-4 Ph stainless steel bar. This allowed for comparison between the fatigue test results carried out on these two sets of samples. Furthermore, the estimated fatigue limits were also compared to the value obtained in another study.

2. Improvement of material integrity: DOE1

Figure 2 details the global optimization process developed to control the part fatigue life by SLM. The SLM process setup parameters considered in this study were: laser power (*LP*), laser travel speed (*LS*), hatch spacing (*HS*) and laser defocusing (*DF*). The first step of this method focused on the improvement of the material integrity (*MI*). The characteristics of the SLM machine (3D System PMX 300) used in the proposed study are: maximum laser power 300 W, maximum laser speed displacement 2,500 mm/s, workspace dimensions 140 mm x 140 mm x 100 mm, N_2 as inert gas and no re-use of the powder, layer thickness size 30 µm. The spreading of the material powder is carried out by a rigid steel roller. With this technology, if the manufactured part deformation is greater than 30 micrometres, the manufacturing process is stopped by the hard collision between the part and the roller. A first set of SLM parameters was therefore defined to improve the Material Integrity (*MI*) using DOE and response surface approaches.

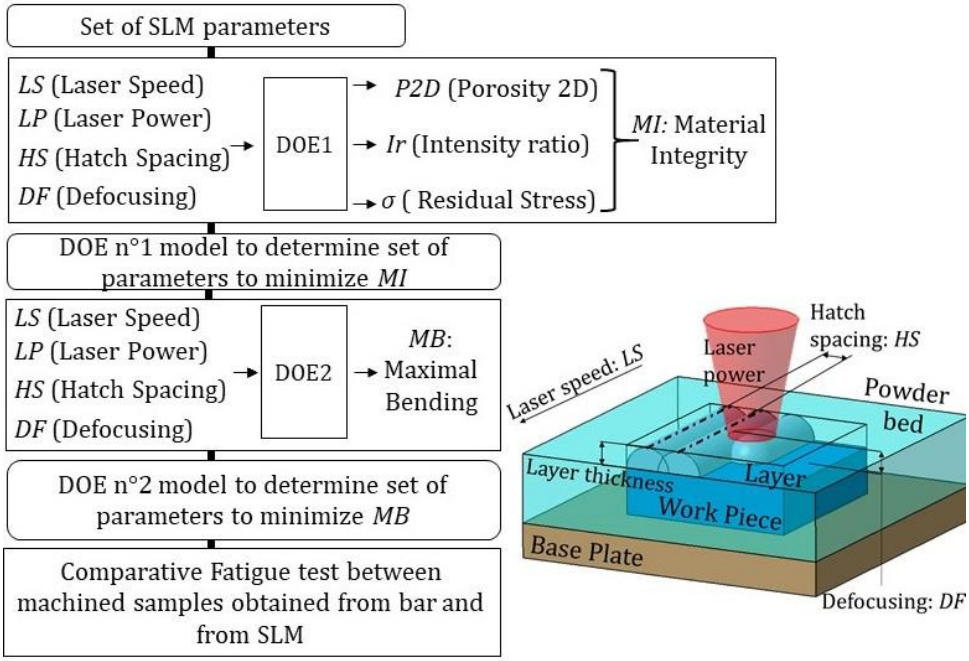

Figure 2 Optimization of SLM setup parameters to control fatigue life.

2.1. DOE1 experimental design

The aim of this first step was to define four SLM process setup parameters *LP*, *LS*, *HS*, and *DF* (figure 2) which provide a great material integrity. Three criteria have been selected and merged to characterize the material integrity *MI*. The first criterion is the residual stress level (σ, see section 2.2). It may induce part geometric deformation and/or crack if the steel elastic limit is locally reached. The second criterion is the ratio (*Ir*, see section 2.3), which characterizes the material crystallographic texture and therefore its mechanical anisotropy. The third criterion, the material porosity degree (*P2D*, see section 2.4) characterises material pores. Material pores are potential crack initiation sites that may reduce the part fatigue life. For this study, we assume that these three criteria have the same weight on the material integrity. Thus, a qualifier (*MI*) of the material integrity was defined by adding the three centred and normalized values of the previous criteria (Equation 1).

$$MI = \frac{\sigma - Mean(\sigma)}{Max(\sigma) - Min(\sigma)} + \frac{Ir - Mean(Ir)}{Max(Ir) - Min(Ir)} + \frac{P2D - Mean(P2D)}{Max(P2D) - Min(P2D)} \qquad (1)$$

A DOE with a spherical experiment domain was employed to determine the effects of *LP*, *LS*, *HS*, and *DF* on *MI*. Indeed, this kind of DOE is adapted to extended domains and has the property of having all the experiments at iso-distance of the centre. For these reasons, this kind of DOE was chosen amongst experimental matrices used in chemometrics, using Nemrodw software (Brown et al., 2020; Lewis et al., 1998) (table 1). This experiment domain is used to derive the response surface to optimize *MI* versus the parameters (*LP*, *LS*, *HS*, and *DF*). Note that, to ensure the orthogonality of all experiments a small radius variation of the domain ($1 \leq$ radius value ≤ 1.25) was introduced by the software in experimental matrix. This kind of DOE has a number of experiments of 21.

The centre of the DOE1 domain was chosen using a previous set of parameters of a similar material, i.e., maraging steel. Indeed, the maraging steel and 17-4 Ph have a martensitic structure. These central point values were *LS* = 1.2 m/s, *LP* = 180 W, *HS* = 60 µm, *DF* = 3. The central experiment (experiments 21 to 23 in table 1) was repeated two times to stabilize the best fit procedure and estimate the experiment standard deviation. 23 cubes were manufactured by SLM machine. For each experiment, the criteria *P2D*, σ and *Ir* were evaluated, and the global qualifier *MI* was derived using equation 1.

N°	LS m/s	LP W	HS µm	DF mm	σ Mpa	Ir	P2D %	MI
1	1.4	180	60	3	370	1.27	0.17	-0.35
2	1	180	60	3	396	1.44	0.19	0.037
3	1.3	207	60	3	435	1.32	0.34	-0.023
4	1.1	153	60	3	544	1.32	0.48	0.25
5	1.3	153	60	3	559	1.33	0.71	0.432
6	1.1	207	60	3	0	1.68	0.52	-0.003
7	1.3	189	68	3	447	1.47	0.39	0.305
8	1.1	171	52	3	317	1.43	0.44	0.026
9	1.3	171	52	3	353	1.37	0.42	-0.028
10	1.2	198	52	3	179	1.34	0.7	-0.231
11	1.1	189	68	3	400	1.42	0.41	0.141
12	1.2	162	68	3	363	1.49	0.27	0.134
13	1.3	189	62	4.6	459	1.26	0.49	-0.023
14	1.1	171	58	1.4	396	1.47	0.43	0.236
15	1.3	171	58	1.4	305	1.42	0.66	0.117
16	1.2	198	58	1.4	209	1.61	0.18	0.019
17	1.2	180	66	1.4	382	1.29	0.22	-0.266
18	1.1	189	62	4.6	189	1.21	0.27	-0.728
19	1.2	162	62	4.6	425	1.16	1.84	0.544
20	1.2	180	54	4.6	211	1.45	0.45	-0.123
21	1.2	180	60	3	296	1.37	0.24	-0.243
22	1.2	180	60	3	355	1.44	0.28	0.029
23	1.2	180	60	3	392	1.27	0.26	-0.253

Table 1 SLM process setup parameters of DOE1 and resulting response.

2.2. Residual stress *(σ)*

A robotic X-Ray stress analyser and its associated software were used to define the residual stress of each sample (on top surface) (figure 3). Its measuring head is equipped with an air-cooled X-Ray tube of 30W and a position sensitive silicon detector offering an angular range of more than 30°. The measurements were carried out in Ψ mounting using Cr Kα radiation. The classical $\sin^2\Psi$ method was employed to evaluate the stresses. 25 Ψ inclinations were used for that purpose.

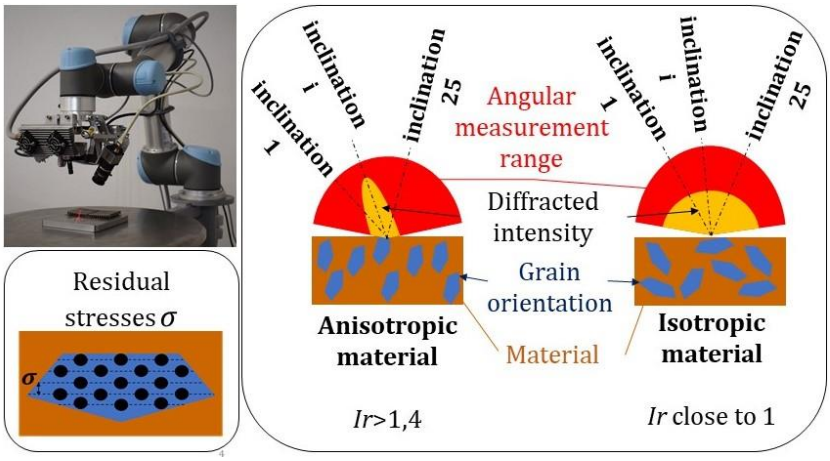

Figure 3 Evaluation of Residual stress and Intensity ratio by X-Ray diffraction.

2.3. Intensity ratio *(Ir)*

The metallurgic state of steel is directly linked to the cooling conditions. SLM induces very high temperature gradients and cooling speeds that lead to dendritic crystallites growing in the direction normal to the surface. This texture causes a strong mechanical anisotropy that is detrimental to fatigue. It can be characterized by the distribution of the X-Ray diffracted intensities measured for different inclinations of the stress analyser head. The ratio (*Ir*) of the maximum to minimum intensity of the diffraction peaks registered during stress evaluations (Equation 2) is thus a good indicator of the material anisotropy degree. The metal can be considered as quasi-isotropic when the factor remains below 1.4.

$$Ir = \frac{Maximum\ diffracted\ intensity}{Minimum\ diffracted\ intensity} \quad (2)$$

2.4. Porosity (P2D)

To characterize the material porosity, the surface of each manufactured cube was machined on 1 mm and then polished. This polishing task was carried out on a NC milling machine with a ball-end polishing tool. In the middle of the polished surface (5mm x 5 mm), a local zone (1.966 mm x 2.621 mm) was measured using an optical microscope. Note that, in order to preserve the polishing tool of the cube edges, the manufactured cube dimensions were 10 mm x 10 mm x 5 mm. This led to obtaining micrographs that were analysed with Image J software to derive the percentage of 2D porosity (figure 4). This procedure was repeated at three different depths (distant of 1 mm each time) on the sample. The mean, maximal, and minimal of the three measured values are summarized in table 2 for each sample. The mean value of three measures was used to characterise the material porosity (*P2D)*.

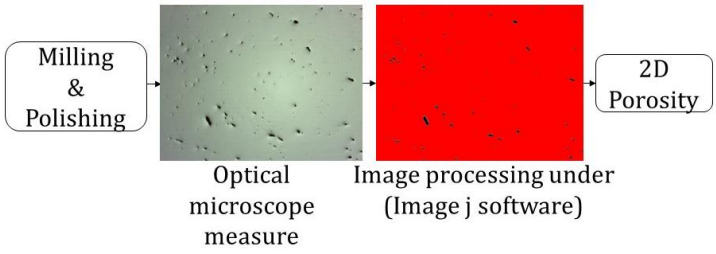

Figure 4 Procedure to characterize the 2D porosity.

Exp	1	2	3	4	5	6	7	8	9	10	11	12
Mean	0.17	0.19	0.34	0.48	0.71	0.52	0.39	0.44	0.42	0.7	0.4	0.27
Min	0.05	0.13	0.05	0.08	0.09	0.2	0.15	0.23	0.21	0.25	0.32	0.18
Max	0.25	0.25	0.87	1.21	1.91	1.05	0.71	0.72	0.58	1.59	0.57	0.36

13	14	15	16	17	18	19	20	21	22	23
0.49	0.43	0.66	0.18	0.22	0.27	1.84	0.45	0.24	0.28	0.26
0.41	0.17	0.16	0.13	0.2	0.26	0.17	0.11	0.18	0.19	0.23
0.63	0.77	1.43	0.2	0.25	0.28	5.11	0.96	0.29	0.41	0.29

Table 2 Experimental values of *P2D*: mean, min, max values versus the experiment number.

2.5 DOE1 results

2.5.1 Response surface model determination

Based on the set of experiments (table 1), the results (material integrity, *MI*) of DOE1 were approximated by a second order polynomial response surface (Equation 3). In this equation, each process setup parameter value has been transformed to a centred and normalized variable, *Xi* (*X*1= *LS*, *X*2 = *LP*, *X*3 = *HS*, *X*4 = *DF*). In this response surface, the number of coefficients is noted *Nf*, and equal to 15.

$$MI = b0 + b1.X1 + b2.X2 + b3.X3 + b4.X4 + b11.X1^2 + b22.X2^2 + b33.X3^2 + b44.X4^2 + b12.X1.X2 + b13.X1.X3 + b14.X1.X4 + b23.X2.X3 + b24.X2.X4 + b34.X3.X4 \quad (3)$$

$$\text{With: } Xi = \frac{2\,.\,(Value\,i\; -\; Mean\,(Value i))}{Max(Value i)\; -\; Min(Value i)} \text{ and } -1 \le Xi \le 1$$

For the determination of the response surface coefficients, vector **B** (*b*0 to *b*34) of equation 3, was estimated using Moore–Penrose inverse method (Courrieu, 2008). This allowed computing the response surface. From this response surface, the optimized setup parameters were derived by a conditional minimization of the global material integrity qualifier *MI* (equation 4). The conditional

minimization was done limiting the *X*i values to comply with the quasi-hyper-spherical experimental domain.

$$\text{Min}(MI) \text{ where } \sqrt{\sum_{i=1}^{Nf} Xi^2} \leq 1.25 \quad (4)$$

The optimized value of *MI* (-0.653) was obtained for the following SLM setup parameters: *LS* = 1.094 m/s, *LP* = 194 W, *HS* = 57 µm, *DF* = 4.5. The hyper-radius for these values is equal to 1.25.

2.5.2 Uncertainty calculation

The associated uncertainty $U(MI)$ also had to be deduced to define the Statistical Confidence Boundaries (Rossi et al., 2014) of the response surface. It required identifying the standard deviation of measured responses *MI* that was defined in two ways. First, the least squares best fit residuals E were derived from the estimated coefficients, as shown in equation 5:

$$\mathbf{E} = \mathbf{MI} - \mathbf{B}.\mathbf{X}$$

where **MI:** vector of *MI* experimental values and **X**: matrix of *X*i and *X*ij values (5)

The standard deviation of these residuals σ_{E} was then computed as shown in equation 6. *Ne* refers to the experiment number, whereas *Nf* refers to the coefficients number and *Em* refers to the residual calculated for experiment *m*. The value of σ_{E} was 0.25.

$$\sigma_{\text{E}} = \sqrt{\frac{1}{N_e - N_f} . \sum_{m=1}^{N_e} E_m^2} \quad (6)$$

As pointed out before, the experiment carried out at the centre of the factor domain was repeated two times. The standard deviation of these three readouts written σ_{exp} was the second way to evaluate the uncertainty bound to the response. The value of σ_{exp} was 0.16. Then, the worse-case scenario ($max(\sigma_E^2; \sigma_{exp}^2)$) was considered. The maximum of these two uncertainties was propagated to derive the variance-covariance matrix of **Cov(B)** as shown in equation 7. The variances of *b*i coefficients were derived from diagonal terms of the matrix **Cov(B)**. $U(b\text{i})$ was obtained using a coverage factor of two: $U(b\text{i}) = k.\sqrt{var(b\text{i})}$, with *k* = 2 (95% of confidence level).

$$\mathbf{Cov}(\mathbf{B}) = (\mathbf{X}^T.\mathbf{X})^{-1}.max(\sigma_E^2; \sigma_{exp}^2) \quad (7)$$

Then, the variance of any estimated point *MI* of the response surface was obtained by propagating the covariance matrix of **B**. The Jacobian of the quadratic model was used for that purpose, as shown in equation 8.

$$var(MI) = \mathbf{J}.\mathbf{Cov}(\mathbf{B}).\mathbf{J^T}$$

With:

$$\mathbf{J} = (1, X1, X2, X3, X4, X1^2, X2^2, X3^2, X4^2, X1.X2, X1.X3, X1.X4, X2.X3, X2.X4, X3.X4) \quad (8)$$

Finally, the uncertainty of a given estimated point *MI*, written $U(MI)$ was obtained using a coverage factor of two: $U(MI) = k.\sqrt{var(MI)}$ with k=2. Table 3 summarizes the *b*i and its uncertainties. Thus, applying the uncertainty computation, the optimized value of *MI* (determined in section 2.5.1) has an uncertainty of ± 0,622.

	MI			*MB*	
	Mean	*U*(*bi*)		Mean	*U*(*bi*)
*b*0	-0.156	0,144	*c*0	2.16	0.035
*b*1	0.009	0.143	*c*1	0.093	0,048
*b*2	-0.228	0.124	*c*2	-0.1	0,048
*b*3	0.075	0.117	*c*3	0.053	0,048
*b*4	-0.055	0.113	*c*4	-0.047	0,048
*b*12	-0.101	0.32	*c*12	-0.026	0,051
*b*13	0.143	0.337	*c*13	-0.022	0,051
*b*14	0.41	0.34	*c*14	0.024	0,051
*b*23	0.266	0.292	*c*23	-0.066	0,051
*b*24	-0.341	0.294	*c*24	0.016	0,051
*b*34	0.223	0.277	*c*34	0.032	0,051
*b*11	-0.001	0.292	*c*11	-0.089	0,128
*b*22	0.32	0.219	*c*22	0.006	0,1276
*b*33	0.143	0.185	*c*33	0.021	0,1276
*b*44	0.048	0.165	*c*44	-0.029	0,1276

Table 3 Estimated coefficient values and its uncertainties of DOE surface response coefficients.

2.5.3 Determination of the best experimental value

Figure 5 shows the calculated *MI* criterion of the 23 experiments, sorted from the smallest to the largest value. The best experiment was number 18 where the experimental value of *MI* was -0.728. For this experiment, the SLM setup parameters were set to *LS* = 1.1 m/s, *LP* = 189 W, *HS* = 62 µm, *DF* = 4.6.

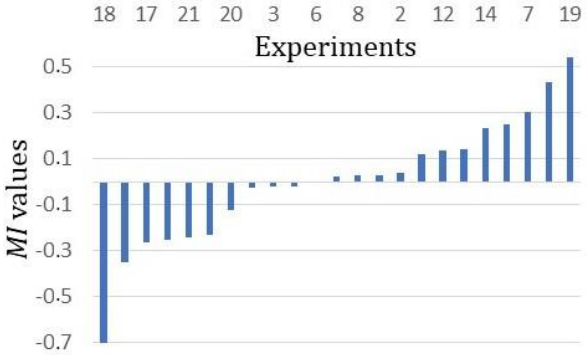

Figure 5 Experimental *MI* values of the 23 experiments.

3. Refining of SLM parameters to reduce residual stress: DOE2

In the first part of our study only surface residual stresses were considered to characterize the material integrity. However, SLM process will also produce in-depth residual stresses that can induce large part deformations and/or crack. Then, the obtained set of SLM process setup parameters at the DOE1 had therefore to be slightly adjusted to reduce the in-depth residual stresses. Furthermore, induced part deformations can stop the manufacturing process, for example, when SLM powder deposition system (steel roller) collides with the last deposited layer.

To quantify the in-depth residual stress, an experiment has therefore been designed to characterize the global effect of residual stresses induced in the deposited material, (Bompos et al., 2020) (figure 6). A beam was thus manufactured on base plate. Cutting most of its supports led to partial residual stress release, causing the beam to bend. This effect was quantified by the maximum deflection noted maximal bending (*MB)*.

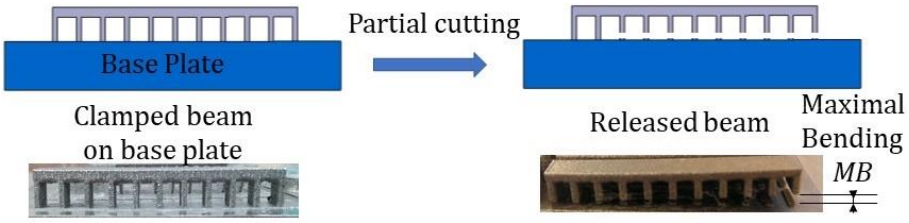

Figure 6 Maximal bending characterization.

MB is an appropriate indicator to describe the in-depth residual stresses existing in the deposited material (figure 6). *MB* was measured using a coordinate measuring machine. To reduce the beam deformation, an additional DOE (DOE2) was carried out to slightly adjust the previous optimum set of SLM setup parameters of the DOE1.

The new DOE2 centre must be chosen in the region where the SLM setup parameters give an optimum *MI* indicator. In the DOE1, experiment 18 has given the lowest result of *MI* (figure 5). Thus, the SLM parameters of experiment number 18 were chosen as centre point for the new DOE. To maintain a great material integrity, local research (DOE2) was done around the centre point. ±5% of SLM parameter variation was applied to include the optimal SLM parameters of previous DOE1. The centre point experiment was repeated three times to estimate the standard deviation and calculate the experimental uncertainties.

3.1 DOE2 experimental design

This DOE was chosen with a cubic experiment domain. DOE2 (25 experiments) required more runs in comparison with the spherical domain (21 experiments) for the same number of parameters. This DOE was generated using Nemrodw software (Brown et al., 2020; Lewis et al., 1998). The setup values of the experiments and resulting *MB* values are shown in table 4. Using these experimental results, a second order polynomial response surface (Equation 9) was derived using the same mathematical method as the DOE1.

$$MB = c0 + c1.X1 + c2.X2 + c3.X3 + c4.X4 + c11.X1^2 + c22.X2^2 + c33.X3^2 + c44.X4^2 + c12.X1.X2 + c13.X1.X3 + c14.X1.X4 + c23.X2.X3 + c24.X2.X4 + c34.X3.X4$$

$$\text{With: } Xi = \frac{2\,.\,(Value\ i - Mean\ (Valuei))}{Max(Valuei) - Min(Valuei)} \text{ and } -1 \leq Xi \leq 1 \qquad (9)$$

3.2 DOE2 results

Table 3 summarizes the *c*i coefficients and its uncertainties. The standard deviation of the measurements (σ_{exp}= 0.06 mm) was also estimated from the four centre point experiments (experiments 25 to 28 in table 4). The standard deviation of the residuals σ_E was 0.102 mm. The worst-case scenario ($max(\sigma_E^2; \sigma_{exp}^2)$) allowed the covariance matrix **Cov(C)** of the coefficients **C**= (c0 to c34) of the response surface polynomial to be assessed.

N°	*LS* [mm/s]	*LP* [W]	*HS* [µm]	*DF* [mm]	*MB* [mm]	N°	*LS* [mm/s]	*LP* [W]	*HS* [µm]	*DF* [mm]	*MB* [mm]
1	1045	180	59	4.4	2.01	15	1045	198	65	4.8	1.89
2	1155	180	59	4.4	2.22	16	1155	198	65	4.8	2.09
3	1045	198	59	4.4	1.95	17	1045	189	62	4.6	1.94
4	1155	198	59	4.4	2.2	18	1155	189	62	4.6	2.2
5	1045	180	65	4.4	2.25	19	1100	180	62	4.6	2.26
6	1155	180	65	4.4	2.49	20	1100	198	62	4.6	2.07
7	1045	198	65	4.4	2.04	21	1100	189	59	4.6	2.21
8	1155	198	65	4.4	1.85	22	1100	189	65	4.6	2.15
9	1045	180	59	4.8	1.88	23	1100	189	62	4.4	2.11
10	1155	180	59	4.8	2.06	24	1100	189	62	4.8	2.15
11	1045	198	59	4.8	1.75	25	1100	189	62	4.6	2.17
12	1155	198	59	4.8	1.99	26	1100	189	62	4.6	2.25
13	1045	180	65	4.8	2.09	27	1100	189	62	4.6	2.28
14	1155	180	65	4.8	2.37	28	1100	189	62	4.6	2.31

Table 4 SLM setup parameters and resulting bending deflection.

Then, conditional minimization of the bending deflection criterion *MB* (Equation 10) led to define the best SLM process parameters.

$$\mathrm{Min}(MB) \text{ where } -1 \leq Xi \leq 1 \qquad (10)$$

The uncertainty $U(MB)$ was derived using the same mathematical method as for the DOE1. The optimum SLM parameters (*LS* = 1.045 m/s, *LP* = 184 W, *HS* = 59 µm, *DF* = 4.8), the related minimum bending deflection *MB* = 1.791mm and its expanded uncertainty $U(MB)$= ±0.165 mm with 95% of confidence level are shown in table 5. To verify the process, two more beams were manufactured by SLM machine:

- The first beam was printed using SLM process setup parameters of the centre point of the domain. A bending deflection *MB* = 2.251 mm was thus measured (table 5).
- The second beam was manufactured using the optimized SLM setup parameters. An experimental maximum deflection *MB* = 1.809 mm was obtained (table 5).

	LS [m/s]	*LP* [W]	*HS* [µm]	*DF* [mm]	*MB* [mm]	
Computation						**Uncertainty**
Parameters to minimize *MB*	1.045	184	59	4.8	**1.791**	**±0.165**
Experimentation						
Central experiment	1.1	189	62	4.6	**2.251**	
Parameters to minimize *MB*	1.045	184	59	4.8	**1.809**	

Table 5 Computation and experimentation results of *MB*.

After determining the SLM parameters, fatigue tests on manufactured samples were performed in order to validate these parameters.

4. Experimental validation of fatigue life

To verify the fatigue strength of the material deposited by SLM machine, five fatigue test specimens were manufactured. These SLM specimens were produced in horizontal position. Additional test samples were also machined from a 17-4Ph stainless steel bar in order to compare the performance of SLM deposited matter to that of a material with high integrity. SLM parts did not present high material quality directly after the deposition phase. It was therefore necessary to add a heat treatment to remove the residual stresses and improve the part metallurgical structure.

3.1 Experimental procedure

Figure 7 shows the manufacturing process of the fatigue test specimens. Five cylindrical samples (Ø14 mm x 110 mm) were first printed with our SLM machine using the optimized parameters: *LS* = 1.045 m/s, *LP* = 184 W, *HS* = 59 µm, *DF* = 4.8.

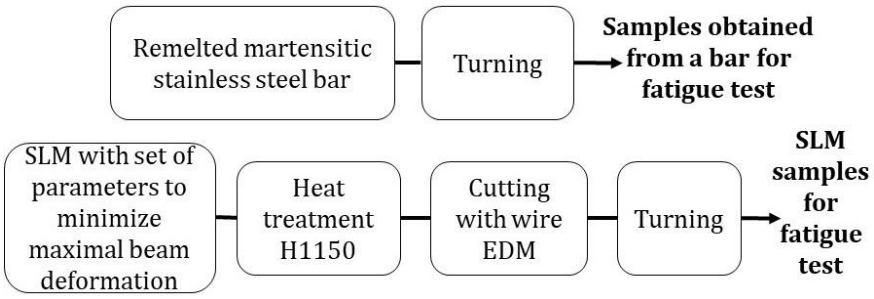

Figure 7 Manufacturing processes to build experimental specimens.

A heat treatment H1150 (heating at 1050°C, oil quenching, annealing for 4 hours at 620°C and air cooling) was then applied to these samples while still bound to the base plate. The specimens were then cut from the base plate by EDM. Standard ISO 1143:2010 fatigue test specimens were finally machined from the raw cylinders by turning. A second set of samples was also manufactured directly from a 17-4Ph stainless steel bar. All the specimens (SLM and machined bars) were machined by the same lathe in the same cutting conditions. They are shown in figure 8. The specimens were finally tested on a rotary bending fatigue machine.

3.2 Experimental validation: fatigue test results

	Fatigue strength (10E7 cycles of fatigue) Mpa	
SLM	471.7 ±38.6	89,88%
Bar	524.8 ±39.0	100%

Table 6 Experimental results of fatigue tests.

Based on the results of the fatigue tests, a statistical model of the matter damage was used to define the SN-Curve of each sample type and estimate the fatigue limit at 10^7 cycles (fracture probability of 50%). The results obtained for the two series of samples are summarized in table 6. The mean value of the fatigue limit and its expanded uncertainty for SLM specimens were evaluated at 471.7 ± 38.6 MPa, and that of machined bars at 524.8 ± 39.0 MPa.

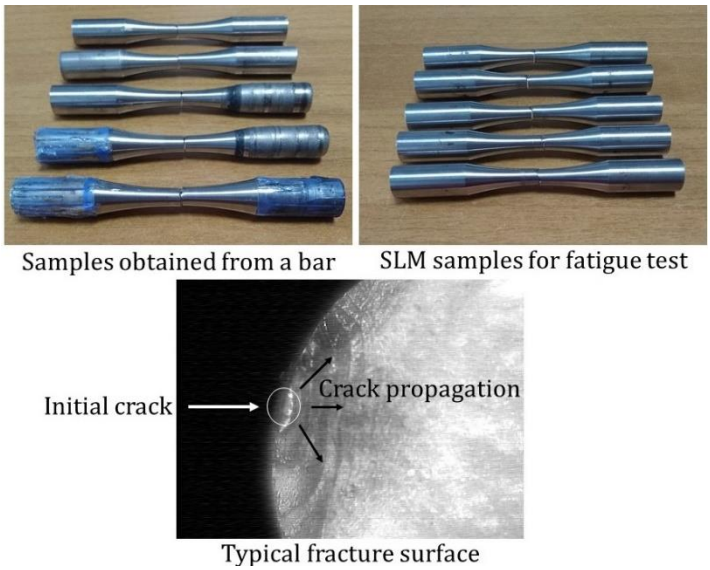

Figure 8 Fatigue test specimens and crack initiation / propagation picture.

4. Discussion

This study showcases the need to determine the SLM parameters to ensure the fatigue life of the 17-4Ph steel. The proposed first DOE aimed to define a draft region of SLM parameters (*LP*, *LS*, *HS*, *DF*) to propose an optimal material integrity (*MI*). *MI* includes sub-criteria: the porosity degree (*P2D*) of the material, residual stress level (σ), and a new one: the material anisotropy, defined by an X-Ray diffracted intensity ratio (*Ir*).

A pie chart (figure 9) has been plotted to discuss the effect of each parameter on the global qualifier *MI*. It shows the relative influence of each model coefficient. To facilitate the readability, the influence percentage of each parameter is displayed in figure 9. This figure highlights that the main contribution in *MI* is provided by the interaction effects, *b*12, *b*13, *b*14, *b*23, *b*24, and *b*34 (62.8%). The *X*i effects, *b*1, *b*2, *b*3 and *b*4 (15.5%) and Xi^2 effects, *b*11, *b*22, *b*33 and *b*44 (21.7%) are lower contribution in *MI*. The exclusive study of Xi effects does not allow us to understand all behaviour of MI. The other effects explain 84.5% of *MI*. This observation confirms the choice of a second-degree response surface model to characterise this complex phenomenon.

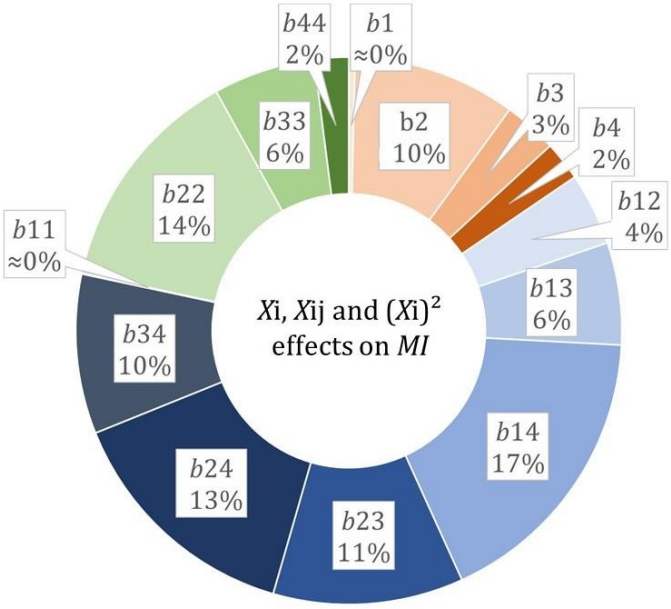

Figure 9 Effect of process parameters on material integrity.

The smallest *MI* value derived from the response surface was -0.653 ± 0.622 (*LS* = 1.094 m/s, *LP* = 194 W, *HS* = 57 µm, *DF* = 4.5). The best experimental value (-0.728) was that of the experiment 18 (*LS* = 1.1 m/s, *LP* = 189 W, *HS* = 62 µm, *DF* = 4.6), it falls within the error bar defined by estimation of *MI* (-1.175 to -0.031).

For the choice of DOE centre for *MB* (DOE2), two sets of SLM parameter values were conceivable: SLM parameters of optimum surface response or those from the DOE1 experiment 18. As shown previously, these two values are very close. To ensure the robustness of the experiments, the SLM parameters of the experiment 18 (table 1) were chosen as DOE2 central value. Furthermore, the DOE2 domain extent was chosen to include the SLM parameters of the optimum *MI* deduced from the DOE1.

A new DOE was done to control the part deformation and to avoid a crack in the material. For this a new criterion named maximum bending *MB* was employed to reduce the residual stress in the produced material. To obtain representative response surface and reduce the experimental uncertainty, a cubic experimental domain was selected to increase the number of experiments (25 experiments) and the experimental domain was thus reduced. This can be verified by the low experimental standard deviation (σ_{exp} = 0.06 mm) and low residuals standard deviation (σ_E = 0.102 mm).

In addition, to validate the reproducibility of SLM machine settings, a comparison between the mean value of four repetitions (25 to 28) of DOE2 central point (2.253 ±0.12 mm) (table 4) and the *MB* value measured in a new experiment using the same SLM parameters was done. The measured experimental *MB* value was 2.251 mm (table 5). This value is close to the mean of the experiments 25 to 28 and within its uncertainty. This result confirms the reproducibility of SLM machine settings.

The optimal SLM parameters were deduced using the DOE2 response surface: *LS* = 1.045 m/s, *LP* = 184 W, *HS* = 59 µm, *DF* = 4.8. The optimal estimated *MB* value was 1.791 ± 0.165 mm. Another experiment was done to check the validity of the optimal SLM parameters given by the response surface. A new test was made using the optimal SLM parameters. The experimental maximum deflection *MB* = 1.809 mm was obtained (table 5). The agreement between these two values confirms that the response surface method has a good capability to estimate the optimum SLM setup parameters. These settings are close to those of experiment 11 which is, among all the tests, the one with the minimum value of MB.

The mean values obtained during the experimental validation of the fatigue control show that the fatigue strength of the specimens manufactured using the SLM optimal parameters (471.7 ± 38.6 MPa at 10^7 cycles) has reached near 90% of the value found for samples machined from a bar (524.8 ± 39.0 MPa) (table 6). This demonstrates the suitability of the method proposed to optimize SLM process and control the fatigue life of 17-4Ph stainless steel. The obtained results can be compared to recent research work (Schneller et al. 2020). This study also presents fatigue test results of 17-4Ph samples manufactured by SLM. The full experimental method was used to derive the fatigue limit of the 17-4 Ph stainless steel. The fatigue limit at 10^7 cycles (fracture probability of 50%) was estimated at 400 MPa after H1150 heat treatment and 450 MPa after Hot Isostatic Pressing (HIP). In another study (Carneiro et al., 2019), a fatigue limit of 300 MPa was obtained for 17-4Ph produced by additive manufacturing. This lower fatigue strength could be partly explained by the difference in quality of the deposited material. It may also be linked to the difference of powder deposition system integrated in the SLM machines used (steamroller in our study, recoater in other studies). Nevertheless, as shown in figure 9, crack initiation sites still exist in the samples manufactured in our study. This could be improved in the future by using HIP treatments.

5. Conclusion

In this study, a Design Of Experiment (DOE) methodology was presented to optimize the Selective Laser Melting (SLM) manufacturing parameters in order to increase the fatigue life of 17-4Ph

stainless steel. A first DOE was used to identify the SLM process parameters that would increase the 17-4Ph material integrity. A second DOE was carried out to reduce the residual stresses in the produced material. The residual stress decrease has two aims: reduce the geometric deformation in order to limit the collisions during manufacturing (recoater and part of workpiece) and avoid crack initiation in the material. Furthermore, fatigue tests were carried out to compare the behaviour of specimens produced by SLM and samples machined from a bar. Contributions of this paper are:

- A methodology was proposed to control the fatigue life of steel material by selecting manufacturing parameters: laser power, laser travel speed, hatch spacing and laser defocusing.
- The correlation between the rate of the laser beam, the laser power, the hatch spacing and the beam defocusing has a significant effect on the material integrity.
- The fatigue limit of SLM samples (produced using optimised parameters) was found to reach near 90% of the fatigue strength of specimens machined from a 17-4Ph steel bar.
- In comparison to a similar study found in the literature (Schneller et al. 2020), the proposed manufacturing parameter optimisation provides an increase of 18% of the fatigue limit at 10^7 cycles.

This work is based on an empirical method, which makes it expensive and time consuming. Future direction of our study would be to develop a numerical approach to predict the quality of the workpiece material to improve the fatigue behaviour.

Acknowledgements

The set of experimental equipment was funded by European Community, French Ministry of Research and Education and Aix-Marseille Conurbation Community. The authors acknowledge AIRBUS Helicopters company for caring out the fatigue tests and MRX company for providing the residual stress analyses.

References

Alnajjar, M., Christien, F., Bosch, C., Wolski, K. (2020), "A comparative study of microstructure and hydrogen embrittlement of selective laser melted and wrought 17–4 PH stainless steel", *Materials Science and Engineering: A*, Vol.785, p.139363. https://doi.org/10.1016/j.msea.2020.139363

Bompos, D., Chaves-Jacob, J., Sprauel, J. M. (2020), Shape distortion prediction in complex 3D parts induced during the selective laser melting process, *CIRP Annals,* Vol.69 N°.1, pp.517-520. https://doi.org/10.1016/j.cirp.2020.04.014

Bourell, D., Kruth, J. P., Leu, M., Levy, G., Rosen, D., Beese, A. M., Clare, A. (2017), "Materials for additive manufacturing", *CIRP Annals,* Vol.66 N°.2, pp.659-681. https://doi.org/10.1016/j.cirp.2017.05.009

Brown, S. D., Tauler, R., Walczak, B. (Eds.). (2020). Comprehensive chemometrics: chemical and biochemical data analysis. Elsevier.

Carneiro, L., Jalalahmadi, B., Ashtekar, A., Jiang, Y. (2019), "Cyclic deformation and fatigue behavior of additively manufactured 17–4 PH stainless steel", *International Journal of Fatigue*, Vol.123, pp.22-30. https://doi.org/10.1016/j.ijfatigue.2019.02.006

Courrieu, P. (2008), "Fast computation of Moore-Penrose inverse matrices". arXiv preprint arXiv:0804.4809.

Dobson, S. D., Starr, T. L. (2021), "Powder characterization and part density for powder bed fusion of 17-4 PH stainless steel". *Rapid Prototyping Journal*. https://doi-org.lama.univ-amu.fr/10.1108/RPJ-01-2020-0023

Gockel, J., Sheridan, L., Koerper, B., Whip, B. (2019), "The influence of additive manufacturing processing parameters on surface roughness and fatigue life", *International Journal of Fatigue*, Vol.124, pp.380-388. https://doi.org/10.1016/j.ijfatigue.2019.03.025

LeBrun, T., Nakamoto, T., Horikawa, K., Kobayashi, H. (2015), "Effect of retained austenite on subsequent thermal processing and resultant mechanical properties of selective laser melted 17–4

PH stainless steel", *Materials & Design*, Vol.81, pp.44-53. https://doi.org/10.1016/j.matdes.2015.05.026

Lewis, G. A., Mathieu, D., Phan-Tan-Luu, R. (1998). Pharmaceutical experimental design. CRC press.

Mahmoudi, M., Elwany, A., Yadollahi, A., Thompson, S.M., Bian, L. Shamsaei, N. (2017), "Mechanical properties and microstructural characterization of selective laser melted 17-4 PH stainless steel", *Rapid Prototyping Journal*, Vol. 23 No. 2, pp. 280-294. https://doi.org/10.1108/RPJ-12-2015-0192

Murr, L. E., Martinez, E., Hernandez, J., Collins, S., Amato, K. N., Gaytan, S. M., Shindo, P. W. (2012), "Microstructures and properties of 17-4 PH stainless steel fabricated by selective laser melting", *Journal of Materials Research and Technology*, Vol.1 N°.3, pp.167-177. https://doi.org/10.1016/S2238-7854(12)70029-7

Nezhadfar, P. D., Shrestha, R., Phan, N., Shamsaei, N. (2019a), "Fatigue behavior of additively manufactured 17-4 PH stainless steel: Synergistic effects of surface roughness and heat treatment". *International Journal of Fatigue*, Vol.124, pp.188-204. https://doi.org/10.1016/j.ijfatigue.2019.02.039

Nezhadfar, P. D., Shrestha, R., Phan, N., Shamsaei, N. (2019b), "Fatigue data for laser beam powder bed fused 17-4 PH stainless steel specimens in different heat treatment and surface roughness conditions". *Data in brief*, Vol.25, p.104215. https://doi.org/10.1016/j.dib.2019.104215

Romano, S., Nezhadfar, P. D., Shamsaei, N., Seifi, M., Beretta, S. (2020), "High cycle fatigue behavior and life prediction for additively manufactured 17-4 PH stainless steel: Effect of sub-surface porosity and surface roughness", *Theoretical and Applied Fracture Mechanics*, Vol.106, 102477. https://doi.org/10.1016/j.tafmec.2020.102477

Rossi, L., Linares, J.M., Chaves-Jacob, J., Mailhé, J. Sprauel, J.M. (2014), "Design optimization using Statistical Confidence Boundaries of response surfaces: Application to robust design of a biomedical implant", *CIRP Annals - Manufacturing Technology* Vol.63, pp.141-144. http://doi.org/10.1016/j.cirp.2014.03.088

Schaller, R. F., Taylor, J. M., Rodelas, J., Schindelholz, E. J. (2017), "Corrosion properties of powder bed fusion additively manufactured 17-4 PH stainless steel", *Corrosion*, Vol.73 N°.7, p.796-807. https://doi.org/10.5006/2365

Schneller, W., Leitner, M., Leuders, S., Sprauel, J. M., Grün, F., Pfeifer, T., Jantschner, O. (2020), "Fatigue strength estimation methodology of additively manufactured metallic bulk material", *Additive Manufacturing*, 101688. https://doi.org/10.1016/j.addma.2020.101688

Schmidt, M., Merklein, M., Bourell, D., Dimitrov, D., Hausotte, T., Wegener, K., Overmeyer, L., Vollertsen, F., Levy, G. N. (2017), "Laser based additive manufacturing in industry and academia", *CIRP Annals*, 66(2), 561-583. https://doi.org/10.1016/j.cirp.2017.05.011

Soltani-Tehrani, A., Pegues, J., Shamsaei, N. (2020), « Fatigue behavior of additively manufactured 17-4 PH stainless steel: The effects of part location and powder re-use", *Additive Manufacturing*, Vol.36, p.101398. https://doi.org/10.1016/j.addma.2020.101398

Tian, Y., Tomus, D., Rometsch, P., Wu, X. (2017), "Influences of processing parameters on surface roughness of Hastelloy X produced by selective laser melting". *Additive Manufacturing*, Vol.13, pp.103-112. https://doi.org/10.1016/j.addma.2016.10.010

Thompson, M. K., Moroni, G., Vaneker, T., Fadel, G., Campbell, R. I., Gibson, I., Bernard, A., Schulz, J., Graf, P., Ahujai, B., Martina, F. (2016), "Design for Additive Manufacturing: Trends, opportunities, considerations, and constraints", CIRP Annals, 65/2:737–760. https://doi.org/10.1016/j.cirp.2016.05.004

Yadollahi, A., Shamsaei, N. (2017), "Additive manufacturing of fatigue resistant materials: Challenges and opportunities". *International Journal of Fatigue*, Vol.98, pp.14-31. https://doi.org/10.1016/j.ijfatigue.2017.01.001

Yadollahi, A., Shamsaei, N., Thompson, S. M., Elwany, A., Bian, L. (2017), "Effects of building

orientation and heat treatment on fatigue behavior of selective laser melted 17-4 PH stainless steel". *International Journal of Fatigue*, Vol. 94, pp.218-235. https://doi.org/10.1016/j.ijfatigue.2016.03.014